Mechanism of Large Magnetostriction of Galfenol

Yanning Zhang and Ruqian Wu

Department of Physics and Astronomy, University of California, Irvine, CA 92697 USA

Galfenol ($\mathrm{Fe}_{100-x}\mathrm{Ga}_x$) and related alloys are very promising new magnetostrictive materials for broad applications. Using the density-functional full-potential linearized augmented plane wave method, we performed systematic theoretical investigations to explore the mechanism that governs the large enhancement of magnetostriction in Galfenol. Here, we review our main theoretical findings on factors that lead to 1) the increase of magnetoelastic coupling; 2) the decrease of the tetragonal shear modulus; and 3) the phase instability. Several ternary FeGaX alloys (X = Zn, Pt, Ir, Ge) were predicted to have large magnetostrictive coefficients, through manipulating electron population and strength of spin-orbit coupling.

Index Terms—**Density functional calculation, galfenol, magnetostriction, spin-orbit coupling.**

I. Introduction

ANISOTROPIC magnetostriction is generally described as the deformation of a body in response to a change in its direction of magnetization through the application of an external magnetic field [1], [2]. Materials with large magnetostrictive coefficients, denoted as $\lambda \propto \Delta l/l$, with l representing the length of a sample and Δl its change, are widely utilized in nanoelectromechanical/microelectromechanical systems, energy harvesters, sensors, actuators, and transducers. On the other hand, materials with extremely small λ are desired in electric transformers, motor shielding, and magnetic recording. Rare-earth based alloys, such as $\mathrm{Tb}_{0.3}\mathrm{Dy}_{0.7}\mathrm{Fe}_{1.92}$ (Terfenol-D), are currently the strongest magnetostrictive materials with $\lambda_{111} > 1000$ ppm (10^{-6}) [3]–[5], but their applications are somewhat limited by several drawbacks such as brittleness, high price, and large operating magnetic field. Intriguingly, Clark *et al.* found that Galfenol, a family of Fe-based alloys with Ga or other metalloid elements, may have strong magnetostriction with $\lambda_{100} \sim$ 100–500 ppm [6]–[10], the highest single crystalline magnetostriction for transition metal alloys. Several unique features characterize the enhanced magnetostrictive behavior of $\mathrm{Fe}_{100-x}\mathrm{Ga}_x$ systems: 1) a quadratically increasing value of λ_{100}, reaching 400 ppm, with increasing x up to 19 in the bcc solid solution; 2) a dramatic shear modulus softening with increasing $x < 27$; 3) a decrease in λ_{100} above $x \approx 20$ and then the reemergence of a second peak in λ_{100} near $x \approx 27$; 4) a sign change in λ_{111} near $x \approx 19$, where λ_{100} reaches its first apex; and 5) an absence of the low-temperature anomaly in λ_{100} that is observed in pure α-Fe. This opens a new vista of achieving strong magnetostriction in ductile metallic materials for a wide range of applications. Extensive interdisciplinary efforts have been dedicated to investigate the mechanism that leads to the large enhancement of magnetostriction, so as to accelerate the development and optimization of functional materials in a timely and cost-effective manner [11]–[14].

Due to its intrinsic complexity, however, magnetostriction in transition metal systems has seldom been tackled theoretically until very recently [15]–[19]. Theoretical studies for Galfenol focused on identifying the key factors, from structural instability, bond modulation, spin-orbit coupling (SOC), to electron population, in order to assist experimental efforts. Recent *ab initio* studies for $\mathrm{Fe}_{100-x}\mathrm{Ga}_x$ $(x < 19)$ and related alloys satisfactorily reproduced experimental results [20]–[22], indicating that the intrinsic electronic structure changes induced by Ga play an essential role. Extrinsic mechanisms such as the field-induced rotation of $\mathrm{D0}_3 - \mathrm{D0}_{22}$ and more recently $\mathrm{B2} - \mathrm{L1}_2$ precipitates have also been proposed as the origin of the large magnetostriction of Galfenol [23]–[25]. However, most single crystalline samples have no obvious phase mixture [13], [26].

Here, we review the background and current status of theoretical studies using the density-functional theory (DFT) for the understanding of magnetostriction in transition metal alloys. In particular, we try to answer several key questions regarding what governs the large magnetostriction in Galfenol and how to further enhance their performance.

II. Methodology

State-of-the-art *ab initio* calculations based on the DFT [27], [28] have been enormously successful, in both explaining existing phenomena and, more importantly, in predicting the properties of new systems. Synergistic applications of theory and experiment, as have been demonstrated repeatedly in many areas of materials science, become a "must" to further advance our understanding of complex materials. The all-electron full-potential linearized augmented plane wave method [29], [30] is known as one of the most accurate and powerful quantum mechanical simulation packages. Here, the wave function, potential, and charge density are expended in a "*natural*" way without artificial shape approximation. The core electrons are treated fully relativistically, while the SOC term is invoked second variationally for the valence states [18].

For a cubic material, the magnetostrictive coefficient can be determined through the strain $(\varepsilon = \Delta l/l_0)$ dependences of

Manuscript received February 21, 2011; accepted May 21, 2011. Date of current version September 23, 2011. Corresponding author: R. Wu (e-mail: wur@uci.edu).

Color versions of one or more of the figures in this paper are available online at http://ieeexplore.ieee.org.

Digital Object Identifier 10.1109/TMAG.2011.2158202

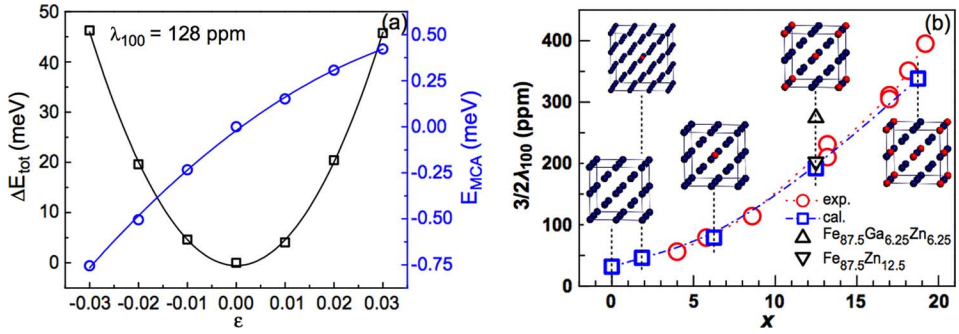

Fig. 1. (a) Calculated strain dependences of $E_{\rm tot}$ (open squares) and $E_{\rm MCA}$ (open circles) of $Fe_{87.5}Ga_{12.5}$. (b) Tetragonal magnetostriction constant $(3/2)\lambda_{100}$ as a function of Ga composition. Circles are the experimental data taken at room temperature [9] and squares are results from the present calculations at 0 K. Triangles show calculated results for $Fe_{87.5}Ga_{6.75}Zn_{6.75}$ and $Fe_{87.5}Zn_{12.5}$, with either one or both Ga being substituted by Zn in the unit cell. Insets are the atomic configurations optimized through the *ab initio* calculations. Blue (red) balls are for Fe (Ga) atoms.

magnetocrystalline anisotropy energy $E_{\rm MCA}$ and total energy $E_{\rm tot}$ as [18]

$$\lambda = \frac{2}{3}\frac{dE_{\rm MCA}/d\varepsilon}{d^2E_{\rm tot}/d\varepsilon^2}. \tag{1}$$

Since $d^2E_{\rm tot}/d\varepsilon^2$ is always positive for stable structures, λ has the same sign as the slope of the $E_{\rm MCA} \sim \varepsilon$ curve. Clearly, the major challenge for the first principles determination of λ is to obtain reliable result of $E_{\rm MCA}$, which is typically very small and requires high accuracy in dealing with the SOC term. In our calculations, $E_{\rm MCA}$ are evaluated through the torque method [18], which can provide stable results with a manageable number of k-points. Benchmark calculations for the cubic bulk Fe, Co, and Ni, and their alloys resulted in a good agreement with experiments [18], [31].

For the convenience of discussions, we recall that the lowest order contribution of SOC toward the total energy is [32]

$$E^{\rm SOC} = -(\xi)^2\Sigma_o\Sigma_u \frac{\left|\langle o|\overrightarrow{\sigma}\cdot\overrightarrow{L}|u\rangle\right|^2}{\varepsilon_u - \varepsilon_o} \tag{2}$$

where o and u represent the sets of occupied and unoccupied states, respectively. For contributions from the d-states, the nonzero matrix elements of the L_z and L_x operators are $\langle xz|L_z|yz\rangle = 1$, $\langle x^2-y^2|L_z|xy\rangle = 2$, $\langle z^2|L_x|xz,yz\rangle = \sqrt{3}$, $\langle xy|L_x|xz,yz\rangle = 1$, and $\langle x^2-y^2|L_x|xz,yz\rangle = 1$.

III. Results and Discussions

An example for the determination of λ_{100} of the binary alloy $Fe_{87.5}Ga_{12.5}$ is illustrated in Fig. 1(a). Both $E_{\rm MCA}$ and $E_{\rm tot}$ are smooth functions of ε along the (100) axis, indicating the high quality of theoretical data. The value of λ_{100} determined with the slope of $E_{\rm MCA}$ and the curvature of $E_{\rm tot}$ at $\varepsilon = 0$ is 128 ppm for $Fe_{87.5}Ga_{12.5}$, in excellent agreement with the experimental data, ~140 ppm [9]. Using this approach, we calculated values of λ_{100} of the ground-state structures of $Fe_{100-x}Ga_x$ alloys $(x < 19)$, as depicted in the insets in Fig. 1(b) [22]. Theoretical results display a quantitative agreement with experiments, good evidence that shows the intrinsic factors as the main sources of large magnetostriction of Galfenol.

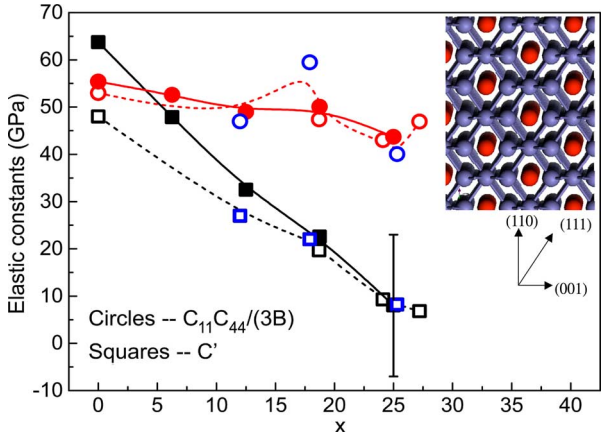

Fig. 2. Calculated and measured values of C' and $(C_{11}C_{44})/(3B)$ for Galfenol. Open and filled symbols denote experimental [9] and theoretical data, respectively. The blue circles and squares are the experimental results from [33]. Curves are for eye guiding. The bar for C' at $x = 25$ indicates the range of theoretical data with slight structural changes. The inset shows the schematic network of Fe–Fe bonds in $Fe_{75}Ga_{25}$ with the $D0_3$ structure viewed from the $(1\bar{1}0)$ direction.

In the regime of $x < 19$, Ga and other metalloid elements affect the properties of Fe by reducing the tetragonal shear modulus C' and enhancing its magnetoelastic coupling coefficient b_1. These lead to a peculiar quadratic behavior of the $\lambda \sim x$ curve of Galfenol before its first peak at $x \sim 19$. It is instructive to separately study the x-dependences of C' and b_1, as well as the phase stability in Galfenol, with systematic DFT calculations.

A. Origin of Lattice Softening in Galfenol

The calculated tetragonal shear modulus C' of Galfenol with $x < 25$ is plotted in Fig. 2, along with results of shear modulus C_{44} that is scaled by a factor of $C_{11}/3B$. Overall, the agreement between theory and experiment is satisfactory in the entire range of Ga concentrations. Notable deviation for C' only occurs near $x = 0$, due to the underestimation of the lattice size of the pure bulk Fe in DFT calculations. It is noteworthy that C_{44} decreases very slightly with x, indicating a strong anisotropic response of the lattice toward external stress.

To understand the mechanism, let us analyze the ordered $D0_3$–$Fe_{75}Ga_{25}$ structure in the inset in Fig. 2, where the pure

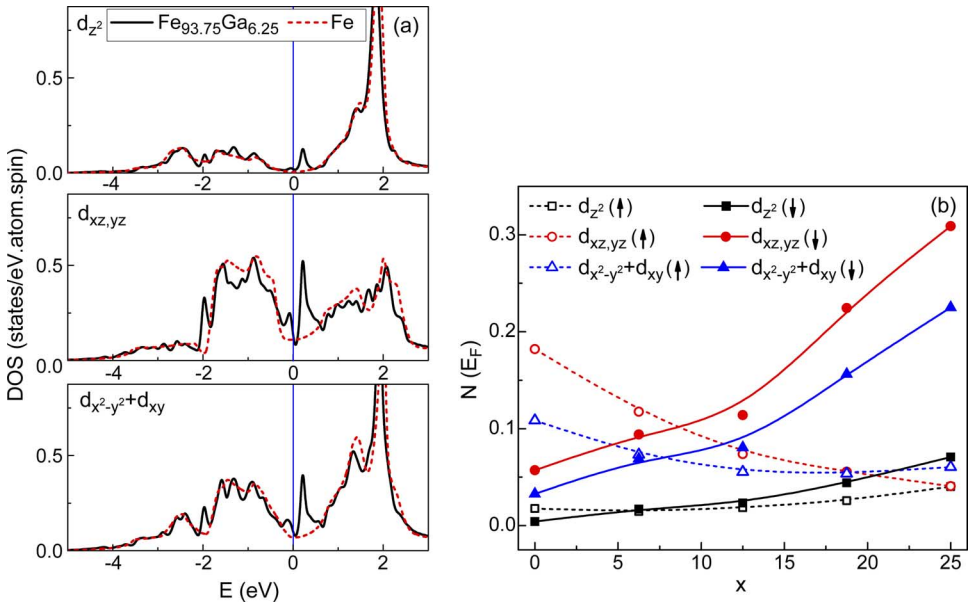

Fig. 3. (a) Projected DOS for different orbitals in the Fe atom nearest to Ga (Fe(C)) in $\mathrm{Fe_{93.75}Ga_{6.25}}$ (solid lines) in the minority spin channel, in comparison to the corresponding results of bulk Fe (dashed lines). The vertical line at $E = 0$ denotes the position of the Fermi level. (b) Number of states around the Fermi level (integrated within ± 0.2 eV) for Fe(C) atoms in $\mathrm{Fe_{100-x}Ga_x}$ $(x < 25\%)$.

Fe layers are alternatively separated by the Fe–Ga mixed layers along the (001) direction. Because of the missing d-orbitals at Ga sites, Fe-bonds toward metalloid atoms become "dangling bonds." With the removal of sticks between Fe and Ga, the network of Fe–Fe bonds is obviously weakened to withstand stress along the (001) axis, which subsequently causes a drastic reduction of C' displayed in Fig. 2. In contrast, the hinge-type network is strong along the (111) direction and, as a result, the value of C_{44} is not much affected by the increase of Ga concentration up to $x = 25$. The large differences between C' and C_{44} of Fe–Ga alloys make them useful as novel auxetic materials that have negative Poisson's ratios when they are stretched along the (110) direction [33].

B. Origin of Magnetoelastic Coupling Enhancement in Galfenol

A simple question one may ask is: which factor is crucial for the large magnetoelastic coupling of Galfenol. The answer at the onset should be "the presence of nonbinding Fe d-states around the Fermi level." According to (1) and (2), an essential feature for strong magnetostrictive materials is to have large E_{MCA} under a small lattice distortion. This can be achieved by reducing the energy separation between occupied and unoccupied states, i.e., the denominator in (2). Fig. 3(a) shows the calculated density of states (DOS) of different d-orbitals in the Fe atom nearest to Ga (denoted by Fe(C) below) in $\mathrm{Fe_{93.75}Ga_{6.25}}$ in the minority spin channel, accompanied by corresponding results of the bulk Fe. The Fe(C) atoms loss their Fe first neighbors and provide more than 70% contributions to the magnetostriction enhancement, particularly from states in the minority spin channel. One obvious observation for the bulk Fe in Fig. 3(a) is that the Fermi level E_{F} lays right at the dip of DOS, and hence, its strain-induced magnetic anisotropy energies are small with large $\varepsilon_u - \varepsilon_o$. The presence of Ga introduces

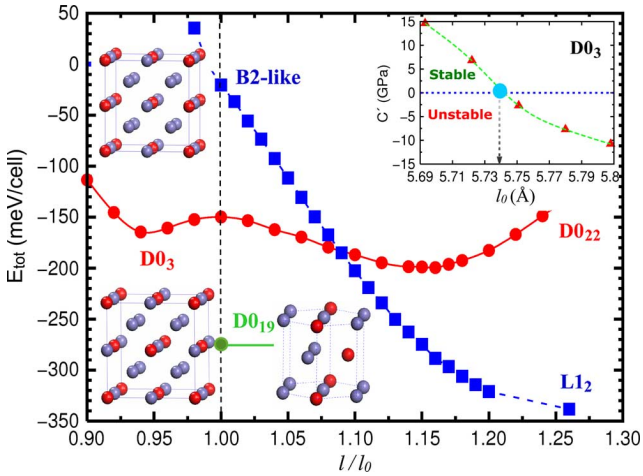

Fig. 4. Strain dependent total energies of the bulk $\mathrm{Fe_{75}Ga_{25}}$ crystal in the B2-like (blue square) and $\mathrm{D0_3}$ (red circle) structures. The green dot indicates the energy of the hexagonal $\mathrm{D0_{19}}$ structure aside. The left insets give the B2-like and $\mathrm{D0_3}$ structures. The right inset shows values of C' for the bulk $\mathrm{D0_3}$–$\mathrm{Fe_3Ga}$ with different lattice sizes.

nonbonding states around Fe(C), mainly with the $d_{xz,yz}$ feature, due to the weak Fe–Ga hybridization. The reduced separation between states across E_{F} significantly enhances their SOC interaction and, hence, the magnetostriction. To further show the correlation between magnetostriction and the availability of Fe(C) d-states around the Fermi level, we give the number of states within ± 0.2 eV in Fig. 3(b) versus the Ga concentration. It is clear that values of $N(E_{\mathrm{F}})$ in the minority spin channel increase monotonically with x, corresponding to the increasing numbers of Fe dangling bonds around Ga atoms. The trend also correlates well to the monotonic increase of magnetostriction in Fig. 1(b). As a further step, one can trace down to the key electronic states that are responsible to the strain dependence of

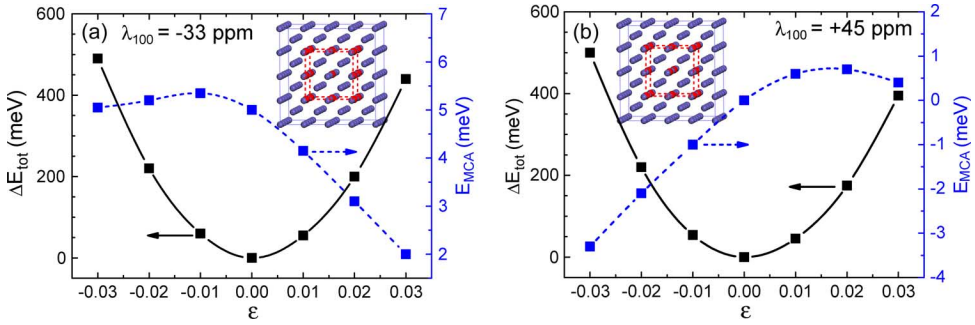

Fig. 5. Schematic cluster models for $Fe_{100-x}Ga_x$ alloys in (a) small B2-like, $x = 11.7$ and (b) $D0_3$-like, $x = 10.9$. Insets are atomic models used in calculations. Blue and red balls are for Fe and Ga atoms, respectively.

E_{MCA}, as we did for B2-like $Fe_{75}Ga_{25}$ [38] and $D0_3$ $Fe_{75}Si_{25}$ [34]. In $Fe_{93.75}Ga_{6.25}$, the Fe(C)–$d_{xz,yz}$ state in the minority spin channel was identified to play the key role in producing large magnetostriction.

C. Structure Stability of Pure Phases of Galfenol

X-ray and neutron diffraction experiments revealed that the first peak in the $\lambda \sim x$ curve of Galfenol associates with the boundary of the A2–$D0_3$ two-phase field [35]. Recent studies demonstrate that quenched Galfenol crystals have mixed phases of A2, B2-like, and $D0_3$ phases at high Ga concentration [36], [37]. Theoretical studies also indicate that the elastic and magnetic properties of Galfenol with $x > 19$ sensitively depend on the local atomic arrangement [38]. Therefore, it is crucial to investigate the energetics and stability of different single crystal phases for the understanding of the dip and the second peak in the $\lambda \sim x$ curve of Galfenol.

For the bcc-type $Fe_{100-x}Ga_x$ crystal structures at $x = 25$, total energies of the B2-like and $D0_3$ phases versus tetragonal lattice distortion are presented in Fig. 4. The total energy of the B2-like structure decreases monotonically as the lattice expands along the z-axis until the fcc-type $L1_2$ arrangement is formed. Interestingly, the $D0_3$ phase of $Fe_{75}Ga_{25}$ is also unstable against the tetragonal distortion, changing toward the fcc-type $D0_{22}$ structure. Nevertheless, the instability of $D0_3$ phase can be contained by various factors such as randomization of a small amount of Ga atoms from their ordered lattice sites as shown by the large change of C' at $x = 25$ in Fig. 2, or by a slight change of the lattice constant. As shown in the inset in Fig. 4, while the $D0_3$–$Fe_{75}Ga_{25}$ bulk has a negative $C' = -3.1$ GPa with the theoretically optimized lattice size ($a = 5.75$ Å), C' changes its sign when the lattice size slightly shrinks by as small as 0.2% to $a = 5.74$ Å. This indicates the high sensitivity of the structural instability of the $D0_3$ phase on the change of local environment.

The field-induced rotation of $D0_3/D0_{22}$ precipitates is the core assumption of the extrinsic mechanism proposed for the explanation of large magnetostriction of Galfenol [23], [24]. We found that the $D0_{22}$ phase is actually higher in energy than the $D0_3$ phase and the metastable structure between them has a c/a ratio of 1.23. Moreover, the hexagonal $D0_{19}$ and cubic $L1_2$ phases are much lower in energy than this $D0_3/D0_{22}$ structure. Experimentally, the precipitation of $L1_2$ phase was observed for some slowly cooled $Fe_{81}Ga_{19}$ sample [39], and it was found

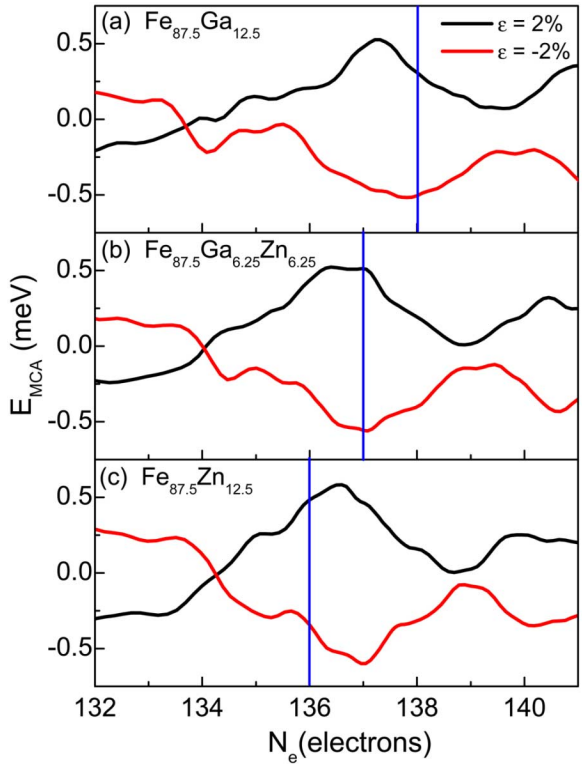

Fig. 6. Calculated E_{MCA} against the band filling N_e for $Fe_{87.5}Ga_{12.5}$, $Fe_{87.5}Ga_{6.25}Zn_{6.25}$, and $Fe_{87.5}Zn_{12.5}$ with $+2\%$ and -2% lattice distortions along the z-axis.

that the $Fe_{73.4}Ga_{25}Ge_{1.6}$ sample, with a small addition of Ge, has two phases: the fcc $L1_2$ and the hexagonal $D0_{19}$, in agreement with our analysis [40], [41]. The observation of elongated $D0_3$-like precipitates in Galfenol samples reported by Cao *et al.* [42] was questioned by more recent studies using X-ray diffuse scattering [36]. The formation of massive $D0_3/D0_{22}$ precipitates should be very unlikely.

We also calculated the equilibrium shape of $D0_3$–$Fe_{75}Ga_{25}$ nanoparticles embedded in Fe or A2 Fe/Ga matrices, using models that contain 128 atoms as shown in the insets in Fig. 5 [43]. No constraint was assumed for the shape and size of the unit cells and all atoms were allowed to relax during the structural optimization procedure. For the structure with B2-like cluster, the entire unit cell expands along the B2-axis (vertical here) but the cluster does not stretch to the $L1_2$ structure as for

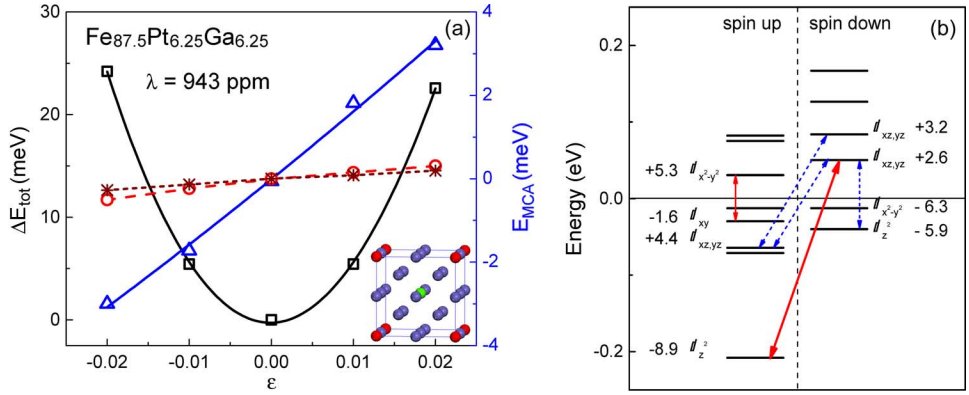

Fig. 7. (a) $E_{\rm tot}$ (open squares) and $E_{\rm MCA}$ (open triangles) of $Fe_{87.5}Pt_{6.25}Ga_{6.25}$ as a function of lattice strain along the z-axis. The open circles (asterisks) with dashed (short-dashed) line represent the strain dependence of $E_{\rm MCA}$ of $Fe_{87.5}Ga_{12.5}$ ($Fe_{93.75}Ga_{6.25}$). The inset is the atomic configuration used in the calculations. (b) Eigenvalues near $E_{\rm F}$ and their wave function features and strain-induced shifts of $Fe_{87.5}Pt_{6.25}Ga_{6.25}$ at Γ point. The solid and dashed arrows highlight the key pairs of states that make positive and negative contributions to $E_{\rm MCA}$, respectively.

the uniform B2-like bulk $Fe_{75}Ga_{25}$. The calculated distance between adjacent Ga atoms is 2.990 Å, a value that agrees well with experimental data extracted from the differential X-ray absorption spectroscopy [44]. Importantly, the $D0_3$-like nanostructure shown in Fig. 5(b) retains its cubic structure in the Fe matrix.

One interesting theoretical finding is the high sensitivity of magnetostriction to the local atomic structure at high Ga concentration ($x \sim 25$). The local B2-like structure was identified to play a key role in the strong positive magnetostriction of Fe–Ga alloys, whereas the $D0_3$ structure provides a negative contribution [38]. Surprisingly, the magnetostrictive coefficients of both B2-like and $D0_3$-like clusters in Fig. 5 are opposite in sign compared to results of their bulk counterparts. For instance, the calculated λ_{100} for the B2-like cluster in Fig. 5(a) is negative, -33 ppm, and λ_{100} for the $D0_3$ cluster in Fig. 5(b) is positive, $+45$ ppm. In Fig. 1, λ_{100} of homogeneous Galfenol samples at $x = 11 \sim 12$ should be around $+120$ ppm. This indicates that the inhomogeneous precipitations are detrimental for the enhancement of magnetostriction.

D. Manipulation of Magnetostriction of Ternary Fe–Ga Alloys

Now we discuss the possibility of using the density-functional approach along with rigid band model for the prediction of magnetostriction in intermetallic alloys. As illustration, the strain ($\varepsilon = \pm 2\%$)-induced magnetic anisotropy energies of $Fe_{87.5}Ga_{12.5}$ are given in Fig. 6(a) versus the number of electrons in the unit cell $N_{\rm e}$. Note that large $E_{\rm MCA}$ at the real $E_{\rm F}$, denoted by the vertical solid lines in Fig. 6, corresponds to strong magnetostriction. It is clear that λ_{100} of $Fe_{87.5}Ga_{12.5}$ can be further enhanced by moving the position of $E_{\rm F}$ over the fixed band structure to the left side, i.e., by taking away about one electron from the unit cell. Practically, this can be done through Zn substitution for Ga, assuming that Ga and Zn behave similarly toward the hybridization with Fe atoms.

To verify the applicability of this approach, DFT calculations were conducted for $Fe_{87.5}Ga_{6.25}Zn_{6.25}$ and $Fe_{87.5}Zn_{12.5}$, by replacing one or two Ga atoms with Zn in the 16-atom cubic unit cell. Interestingly, the three sets of $E_{\rm MCA}(N_{\rm e})$ curves in Fig. 6 are very similar. The $E_{\rm F}$ of $Fe_{87.5}Ga_{6.25}Zn_{6.25}$ locates right at the peaks of the $E_{\rm MCA}(N_{\rm e})$ curves in Fig. 6(b), which leads to $\lambda_{100} = 183$ ppm, 43% larger than that of $Fe_{87.5}Ga_{12.5}$. Further reduction of $N_{\rm e}$ decreases λ_{100} to 134 ppm for $Fe_{87.5}Zn_{12.5}$. DOS curves indicate that substitution of Zn for Ga mainly causes band shift against $E_{\rm F}$ but hardly changes the band structure. Therefore, the applicability of the rigid band model can be established for the prediction of magnetostriction of Galfenol and related alloys in a reasonable range of $N_{\rm e}$. Fundamentally, changing $N_{\rm e}$ alters the leading pairs of states across the Fermi level and permits to capture those with strong SOC interaction.

Another way one can use to control magnetostriction is the SOC matrix elements in (2). Some heavy elements, such as Pt and Ir, are good providers of large SOC as found in perpendicular magnetic recording media [45]. To demonstrate the importance of large SOC on magnetostriction, we give $E_{\rm MCA}$–ε curve of $Fe_{87.5}Pt_{6.25}Ga_{6.25}$ in Fig. 7(a), together with results of $Fe_{93.75}Ga_{6.25}$ and $Fe_{87.5}Ga_{12.5}$. While the calculated $E_{\rm MCA}$ of the distorted $Fe_{87.5}Pt_{6.25}Ga_{6.25}$ structure ($\varepsilon = 2\%$) is over 3 meV/cell, the corresponding values of Fe–Ga binary alloys are only ~0.45 meV/cell. In addition, $E_{\rm MCA}$ and λ_{100} of $Fe_{87.5}Pt_{6.25}Ga_{6.25}$ drop by a factor of seven if we selectively switch off the SOC of Pt in calculations. It is also striking to find that λ_{100} of $Fe_{87.5}Pt_{6.25}Ga_{6.25}$ becomes unusually high, $+943$ ppm, a value that is $2 \sim 3$ times higher than the best magnetostrictive coefficient of binary Galfenol alloys reported so far. With the same configuration model, the calculated λ_{001} of $Fe_{87.5}Pt_{6.25}Al_{6.25}$ is also as high as $+1156$ ppm. Calculations with other elements and compositions suggest that many ternary alloys may have giant magnetostriction, $|\lambda_{100}| > 1000$ ppm. For example, a $Fe_{75}Pt_{6.25}Ge_{18.75}$ model structure has $|\lambda_{100}|$ up to 3500 ppm, even larger than that of Terfenol-D ($\lambda_{111} \sim 1600$ ppm). Although the hypothetical structural model might be too simple for complex ternary alloys, these results conceptually indicate a possibility of making strongly magnetostrictive materials through appropriately combined actions of Pt that provides large SOC, and Ga (or other metalloid elements) that weakens the d-states of adjacent Fe.

We further found that the "hot" zone of $Fe_{87.5}Pt_{6.25}Ga_{6.25}$ to the magnetostriction is round the Γ point. To appreciate roles

of different electronic states, we give all eigenstates near the Fermi level (± 0.2 eV) at the Γ point in Fig. 7(b) and highlight the key pairs of occupied and unoccupied states with arrows. The d_z^2 states in both the majority and minority spin channels play important roles in producing large enhancement of $E_{\rm MCA}$, mainly through the $\langle xz \downarrow |\xi L_x| z^2 \downarrow\rangle$ and $\langle xz \downarrow |\xi L_x| z^2 \uparrow\rangle$ pairs, couplings across $E_{\rm F}$ (the up and down arrows denote the majority and minority spins, respectively). Because of the strong mixing between Fe–d and Pt–d_z^2 states, these matrix elements are much larger than those in binary Fe–Ga alloys. Moreover, the energy positions of these states, i.e., ε_o and ε_u in (2), are sensitive to the tetragonal lattice distortions since the d_z^2 states point directly along the (001) axis. Quantitatively, the direction and magnitude of strain-induced energy shifts are also given in Fig. 7(b) for different states around $E_{\rm F}$. It is obvious that eigenenergies of the d_z^2 states change much faster (about two times) than other states under lattice distortions.

IV. Summary

Extensive density-functional calculations provide insightful understandings of the large enhancement of magnetostriction of Galfenol and related alloys. Satisfactory agreements between theory and experiment have been achieved for the determination of elastic and magnetoelastic properties of Galfenol at low Ga concentration. We demonstrated that the large magnetostriction of Galfenol is caused by intrinsic electronic properties, rather than by the formation of heterogeneous precipitations or nanoparticles. Further analysis using the rigid band model indicates that one can enhance magnetostriction of Galfenol by substituting Ga with Zn or Ge, or by substituting Fe with Pt or Ir. Clearly, density-functional studies are useful to address the most fundamental issues regarding magnetostriction in intermetallic alloys, and to provide instructive guideline for the further development of the magnetostrictive materials.

Acknowledgment

We are indebted to insightful discussions with Drs. A.E. Clark, M. Wun-Fogle, K.B. Hathaway, T. Lograsso, and A.B. Flatau. This work was supported by the Office of Naval Research under Grant N00014-08-1-0143 and calculations were conducted on DoD supercomputers.

References

[1] M. R. J. Gibbs, *Modern Trends in Magnetostriction Study and Application*. Boston, MA: Kluwer, 2001.
[2] G. Engdahl, *Handbook of Giant Magnetostrictive Materials*. San Diego, CA: Academic, 2002.
[3] A. E. Clark, *Ferromagnetic Materials*, E. P. Wohlfarth, Ed. Amsterdam, The Netherlands: North Holland, 1980, p. 531.
[4] J. P. Teter, M. Wun-Fogle, A. E. Clark, and K. Mahoney, *J. Appl. Phys.*, vol. 67, p. 5004, 1990.
[5] L. Sandlund, M. Fahlander, T. Cedell, A. E. Clark, J. B. Restorff, and M. Wun-Fogle, *J. Appl. Phys.*, vol. 75, p. 5656, 1994.
[6] S. Guruswamy, N. Srisukhumbowornchai, A. E. Clark, J. B. Restorff, and M. Wun-Fogle, *Scr. Mater.*, vol. 43, p. 239, 2000.
[7] A. E. Clark, J. B. Restorff, M. Wun-Fogle, T. A. Lograsso, and D. L. Schlagel, *IEEE Trans. Magn.*, vol. 36, p. 3238, 2000.
[8] A. E. Clark, M. Wun-Fogle, J. B. Restorff, and T. A. Lograsso, *IEEE Trans. Magn.*, vol. 37, p. 2678, 2001.
[9] A. E. Clark, K. B. Hathaway, M. Wun-Fogle, J. B. Restorff, T. A. Lograsso, V. M. Keppens, G. Petculescu, and R. A. Taylor, *J. Appl. Phys.*, vol. 93, p. 8621, 2003.
[10] J. R. Cullen, A. E. Clark, M. Wun-Fogle, J. B. Restorff, and T. A. Lograsso, *J. Magn. Magn. Mater.*, vol. 226–230, p. 948, 2001.
[11] E. M. Summers, T. A. Lograsso, and M. Wun-Fogle, *J. Mater. Sci.*, vol. 42, p. 9582, 2007.
[12] J. R. Cullen, P. Zhao, and M. Wuttig, *J. Appl. Phys.*, vol. 101, p. 123922, 2007.
[13] Q. Xing, Y. Du, R. J. McQueeney, and T. A. Lograsso, *Acta. Mater.*, vol. 56, p. 4536, 2008.
[14] Q. Xing and T. A. Lograsso, *Appl. Phys. Lett.*, vol. 93, p. 182501, 2008.
[15] R. Q. Wu and A. J. Freeman, *J. Appl. Phys.*, vol. 79, p. 6209, 1996.
[16] R. Q. Wu, L. J. Chen, and A. J. Freeman, *J. Magn. Magn. Mater.*, vol. 170, p. 103, 1997.
[17] R. Q. Wu, L. J. Chen, and A. J. Freeman, *J. Magn. Magn. Mater.*, vol. 177, p. 1216, 1998.
[18] R. Q. Wu and A. J. Freeman, *J. Magn. Magn. Mater.*, vol. 200, p. 498, 1999.
[19] R. Q. Wu, Z. X. Yang, and J. S. Hong, *J. Phys.: Condens. Matter*, vol. 15, p. S587, 2003.
[20] S. C. Hong, W. S. Yun, and R. Q. Wu, *Phys. Rev. B*, vol. 79, p. 054419, 2009.
[21] J. X. Cao, Y. N. Zhang, W. J. Ouyang, and R. Q. Wu, *Phys. Rev. B*, vol. 80, p. 104414, 2009.
[22] Y. N. Zhang, J. X. Cao, and R. Q. Wu, *Appl. Phys. Lett.*, vol. 96, p. 062508, 2010.
[23] A. G. Khachaturyan and D. Viehland, *Metall. Mater. Trans. A*, vol. 38, p. 2308, 2007.
[24] A. G. Khachaturyan and D. Viehland, *Metall. Mater. Trans. A*, vol. 38, p. 2317, 2007.
[25] J. Boisse, H. Zapolsky, and A. G. Khachaturyan, *Acta Mater.*.
[26] M. Huang and T. A. Lograsso, *Appl. Phys. Lett.*, vol. 95, p. 171907, 2009.
[27] P. Hohenberg and W. Kohn, *Phys. Rev.*, vol. 136, p. 864, 1964.
[28] W. Kohn and L. J. Sham, *Phys. Rev.*, vol. 140, p. 1133, 1965.
[29] E. Wimmer, H. Krakauer, M. Weinert, and A. J. Freeman, *Phys. Rev. B*, vol. 24, p. 864, 1981.
[30] M. Weinert, E. Wimmer, and A. J. Freeman, *Phys. Rev. B*, vol. 26, p. 4571, 1982.
[31] Q. Xing, T. A. Lograsso, M. P. Ruffoni, C. Azimonte, S. Pascarelli, and D. J. Miller, *Appl. Phys. Lett.*, vol. 97, p. 072508, 2010.
[32] D. Wang, R. Wu, and A. J. Freeman, *Phys. Rev. B*, vol. 47, p. 14932, 1993.
[33] Y. N. Zhang, R. Q. Wu, H. M. Schurter, and A. B. Flatau, *J. Appl. Phys.*, vol. 108, p. 023513, 2010.
[34] Y. N. Zhang, J. X. Cao, I. Barsukov, J. Lindner, B. Krumme, H. Wende, and R. Q. Wu, *Phys. Rev. B*, vol. 81, p. 144418, 2010.
[35] T. A. Lograsso, A. R. Ross, D. L. Schlagel, A. E. Clark, and M. Wun-Fogle, *J. Alloys Comp.*, vol. 350, p. 95, 2003.
[36] Y. Du, M. Huang, S. Chang, D. L. Schlagel, T. A. Lograsso, and R. J. McQueeney, *Phys. Rev. B*, vol. 81, p. 054432, 2010.
[37] N. Mehmood, R. Sato Turtelli, R. Grössinger, and M. Kriegisch, *J. Magn. Magn. Mater.*, vol. 322, p. 1609, 2010.
[38] R. Q. Wu, *J. Appl. Phys.*, vol. 91, p. 7358, 2002.
[39] J. Zhang, T. Ma, and M. Yan, *Physica B*, vol. 405, p. 3129, 2010.
[40] G. Petculescu, K. L. Ledet, M. Huang, T. A. Lograsso, Y. N. Zhang, R. Q. Wu, M. Wun-Fogle, J. B. Restorff, A. E. Clark, and K. B. Hathaway, *J. Appl. Phys.*, vol. 109, p. 07A904, 2011.
[41] G. Petculescu, A. O. Mandru, W. M. Yuhasz, T. A. Lograsso, M. Wun-Fogle, J. B. Restorff, A. E. Clark, and K. B. Hathaway, *J. Appl. Phys.*, vol. 107, p. 09A926, 2010.
[42] H. Cao, P. M. Gehring, C. P. Devreugd, J. A. Rodriguez-Rivera, J. Li, and D. Viehland, *Phys. Rev. Lett.*, vol. 102, p. 127201, 2009.
[43] H. Wang, Y. N. Zhang, T. Yang, Z. D. Zhang, L. Z. Sun, and R. Q. Wu, *Appl. Phys. Lett.*, vol. 97, p. 262505, 2010.
[44] M. P. Ruffoni, S. Pascarelli, R. Grössinger, R. Sato Turtelli, C. Bormio-Nunes, and R. F. Pettifer, *Phys. Rev. Lett.*, vol. 101, p. 147202, 2008.
[45] D. Weller, A. Moser, L. Folks, M. E. Best, W. Lee, M. F. Toney, M. Schwickert, J.-U. Thiele, and M. F. Doerner, *IEEE Trans. Magn.*, vol. 36, p. 10, 2000.